EBSD characterization of Al7075/graphene nanoplates/carbon nanotubes composites processed through post-deformation annealing

Imanian Ghazanlou, Siavash; Eghbali, Baitallah; Petrov, Roumen

DOI
10.1016/S1003-6326(21)65652-2

Publication date
2021

Document Version
Final published version

Published in
Transactions of Nonferrous Metals Society of China (English Edition)

Available online at www.sciencedirect.com
ScienceDirect
Trans. Nonferrous Met. Soc. China 31(2021) 2250−2263
Transactions of Nonferrous Metals Society of China
www.tnmsc.cn

EBSD characterization of Al7075/graphene nanoplates/carbon nanotubes composites processed through post-deformation annealing

Siavash IMANIAN GHAZANLOU[1], Baitallah EGHBALI[1], Roumen PETROV[2,3]

1. Faculty of Materials Engineering, Sahand University of Technology, P. O. Box: 51335-1996, Tabriz, Iran;
2. Department of Electromechanical Systems and Metal Engineering, Research Group Materials Science and Technology, Ghent University, Tech Lane Science Park Campus A, 46, 9062 Gent, Belgium;
3. Department of Materials Science and Engineering, Delft University of Technology, Mekelweg 2, Delft, The Netherlands

Received 23 August 2020; accepted 4 February 2021

Abstract: The effects of the post-deformation annealing on the microstructural evolution of hot rolled Al7075 matrix composites reinforced with CNTs and GNPs were investigated. The multi-pass hot rolling was applied on the stir cast samples. Annealing was then applied to the composites at 450 °C for 4 h. Microstructural evolution was examined by SEM, EDS, and EBSD techniques. EBSD data showed that the addition of 0.87 vol.% (GNPs + CNTs) significantly inhibited the occurrence of recrystallization. Also, in the composite with 0.96 vol.% CNTs, recrystallization was partially inhibited. Whereas, in composites with 0.92 vol.% of GNPs, the occurrence of recrystallization through particle stimulated nucleation (PSN) mechanism was significantly accelerated. The volume fraction of recrystallized grains depends significantly on the occurrence of PSN in the presence of reinforcements. The intensity and type of the main components of the texture as well as the FCC fibers depend on the type of reinforcement.

Key words: annealing; composite; graphene nanoplates; carbon nanotubes; recrystallization; particle stimulated nucleation; texture

1 Introduction

Today, research on metal matrix composites (MMCs), especially aluminum matrix composites (AMMCs), has increased due to favorable mechanical and physical properties such as lightweight, good thermal and electrical conductivity, good corrosion and wear, and low thermal expansion coefficient. These features make AMMCs attractive to many applications [1,2]. MMCs can be produced through various methods such as electrochemical deposition as surface coating [3−5], compocasting, powder metallurgy and agitator casting. Preparation of MMCs through these techniques is associated with problems such as porosity formation, particle agglomeration, and adverse chemical reaction at the particle/matrix interface which reduces their mechanical properties [6,7].

To eliminate the mentioned problems, the use of hot rolling and severe plastic deformation (SPD) methods such as accumulative roll bonding (ARB), equal channel angular pressure (ECAP) and torsional extrusion (TE) has been proposed [1,8−12]. As reported [13,14], applying plastic deformation to the Al matrix composite containing CNTs can lead to uniform dispersion of CNTs in the matrix. Also, plastic deformation improves CNTs/Al interfacial bonding and eliminates porosity created during casting. In addition, it has been reported that due to the plastic

Corresponding author: Baitallah EGHBALI, E-mail: eghbali@sut.ac.ir
DOI: 10.1016/S1003-6326(21)65652-2

deformation, CNTs clusters are broken and CNTs orientations change [13,15,16]. It has been seen that plastic deformation through the ARB also reduces the size of CNTs reinforcements [16]. Recently, interest in the graphene-reinforced MMCs has increased due to their good electrical [17], mechanical [18] and thermal [19] properties.

AMMCs containing graphene composites have been extensively studied. To prepare graphene-reinforced AMMCs, various techniques such as cryomilling followed by hot extrusion [20] and wet ball mill with hot press [21] have been used.

It has been reported that hot rolling of AMMCs containing GNPs resulting from powder metallurgy leads to 30% increase in composite hardness [22]. Our studies show that to date no significant studies have been performed on the effect of post-deformation annealing on the microstructure evolution of CNTs and GNPs reinforced aluminum matrix composites.

Accordingly, in the present study, the effects of post-deformation annealing on the microstructural evolution of hot-rolled Al7075 matrix composites reinforced with CNTs and GNPs were investigated. Also, the occurrence of PSN at the interface of reinforcement/matrix and the effect of the separate and simultaneous presence of CNTs and GNPs on texture evolution in post-deformation annealed composites were investigated.

2 Experimental

In the present study, Al7075 alloy was used as the matrix material with the chemical composition listed in Table 1. Figure 1 shows the electron microscopic micrographs of CNTs and GNPs reinforcements used in this work.

Table 1 Chemical composition of Al7075 alloy (wt.%)

Al	Zn	Mg	Cu	Fe	Cr	Mn	Ti	Pb, Sn, Si, Ni
89.11	5.89	2.19	1.53	0.26	0.22	0.20	0.13	Bal.

Al7075 matrix composites with different amounts of CNTs and GNPs reinforcements were produced by stirring casting process. Table 2 shows the types of composites obtained from stir casting. Because both CNTs and GNPs are made of carbon,

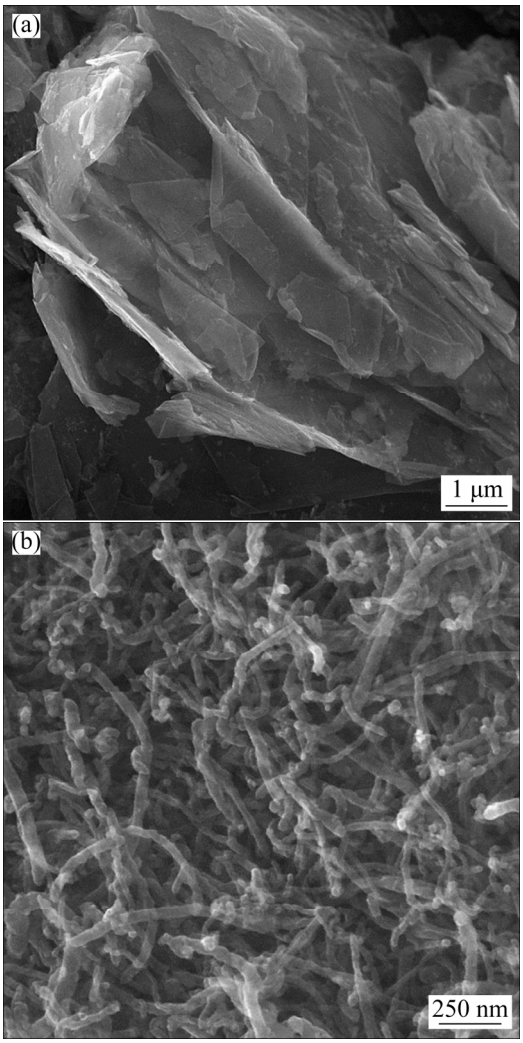

Fig. 1 SEM images of graphene nano-plates (GNPs) (a) and carbon nano-tubes (CNTs) (b)

Table 2 Content of reinforcements in composites

Specimen No.	Content of reinforcement
1	0
2	0.92 vol.% GNPs
3	0.96 vol.% CNTs
4	0.87 vol.% (CNTs+GNPs) (with an equal volume ratio of reinforcements)

the volume fraction of carbon in the samples was measured using a carbon and sulfur analyzer, which is the most accurate carbon analyzer. Using EDX to measure carbon is not accurate because carbon is a light element and cannot be accurately quantified by EDX. During stir casting, the ingot temperature was first raised to 650 °C. The molten metal was mixed using a blade at 350 r/min. CNTs/GNPs reinforcements were mixed with powdered

aluminum at 70 r/min for 3 h. A mixture of reinforcements and aluminum powder (approximately 20 μm) was then injected into the molten Al7075 via argon gas. The slurry temperature was raised to 790 °C. Then, the resulting mixtures were poured into a steel mold beneath the alumina crucible. The cast composites were cut in length, width and thickness of 100 mm × 60 mm × 20 mm.

In the following, the annealing was performed at 450 °C for 4 h on the cast samples and then subjected to multi-pass hot rolling. Hot rolling was performed up to 10 passes at 450 °C until a 95% reduction in total thickness was achieved. The hot rolled composites were annealed at 450 °C for 4 h after deformation at 450 °C for 4 h.

For scanning electron microscope (SEM), energy dispersive spectroscopy (EDS), and electron backscatter diffraction (EBSD) characterizations, the samples were abraded using sandpaper (from grades of 100 to 4000) followed by polishing with diamond paste up to 1 μm along with colloidal silica with size of 0.035 μm. FEI Quanta 450 FEG-SEM equipped with orientation image microscopy (OIM) was used for microstructure analysis of rolling direction−normal direction (RD−ND section). TSL OIM EBSD analysis software package was used to analyze the EBSD patterns. Lower and higher magnifications of EBSD analysis were obtained using scan stage sizes of 1 and 0.3 μm, respectively. The confidence index (CI) was >0.1 for all samples, if otherwise, the whole sample preparation and EBSD measurements were repeated again. A “clean-up” post processing took place in one or two steps, after EBSD measurement. In low magnifications, according to CI standardization (CI>0.1, grain tolerance angle 5°, minimum grain size 2 μm), the EBSD clean-up was done. Later, the neighbor orientation correlation took place (clean up level 4). CI standardization (CI>0.1, grain tolerance angle 5°, minimum grain size 2 μm) was also used for the EBSD clean-up process at higher magnifications. According to the ASTM standard, the Brinell hardness method was used to measure the hardness of composites made in the RD−TD section, which was performed using a 2.5 mm-diameter steel ball with a load of 312.5 N for 15 s. On average, 10 hardness measurements were considered as the final hardness of the samples.

3 Results and discussion

3.1 Microstructure characterization

3.1.1 EDS analysis and SEM images

Figure 2 shows the results of EDS analysis of post-deformation annealed samples with different volume fractions of reinforcement. This analysis shows that the second phase Al_XFe particles (X: 3, 6) are present in the matrix of all processed composites (white particles). CNTs and GNPs clusters are also seen in the black and elongated shape phases.

Figure 3 shows the SEM images of the post-deformation annealed samples. In composite samples, in addition to the distribution of Al_XFe particles (X: 3, 6), parallel scattering of clustered CNTs and GNPs is observed in the matrix. According to the SEM analysis of the as-cast composites made in our previous research [23], cluster CNTs and GNPs were irregular. In addition, the second phases (Al_2Cu particles) and reinforcements were randomly distributed in the matrix.

3.1.2 EBSD analysis on recrystallization of ARBed composites

Figure 4 shows the inverse pole figure (IPF) maps from the ND–RD sections of the post-deformation annealed composites.

As shown in Fig. 4, the average grain sizes (grains with misorientation angle greater than 15 °) of Al7075, 0.92 vol.% GNP, 0.96 vol.% CNTs, 0.87 vol.% (CNTs+GNPs) composites are about 55, 28, 32, and 31 μm, respectively. After the post-deformation annealing, in the hybrid composite most of the grains were still elongated in the roll direction. This indicates that recrystallization is prevented in hybrid composites due to the simultaneous presence of CNTs+GNPs and the elongated morphology of the deformed grains has not changed much. But in other composites, the morphology of the grains is more equiaxed than that of the hybrid composite, and this may be due to the occurrence of recrystallization in them. The orientation gradient shown as the color change in the grains in Fig. 4(d) as evidence, shows that recrystallization has been prevented. Such gradients are not well present in the other IPF maps and they are completely missing in the sample without reinforcement (Fig. 4(a)). These assumptions were

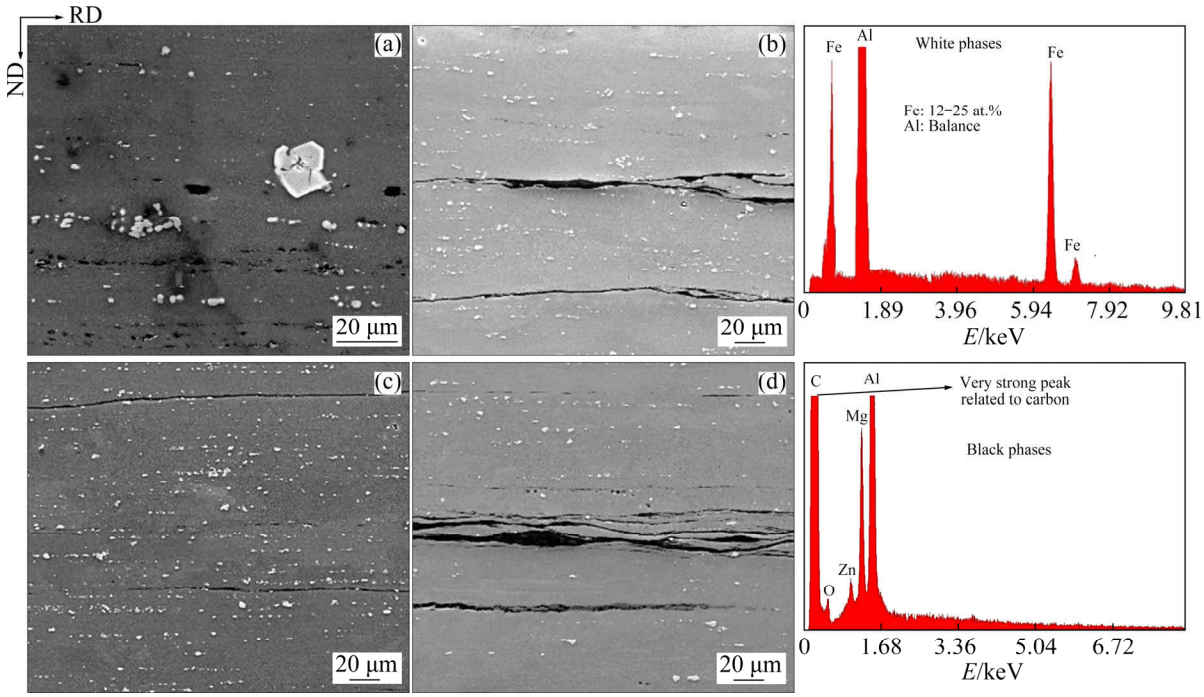

Fig. 2 EDS analysis of ND–RD sections of post-deformation annealed Al7075 matrix composites with different volume fractions of reinforcements: (a) 0; (b) 0.92 vol.% GNPs; (c) 0.96 vol.% CNTs; (d) 0.87 vol.% (CNTs+ GNPs)

supported using grain orientation spread (GOS) maps and GOS graphs that were represented in Figs. 5 and 6, respectively. GOS technique is used to identify the recrystallized grains from the unrecrystallized ones. Because the recrystallized grains are strain-free, their GOS value is low. The threshold value for the GOS degree to recognize the recrystallized grains from the unrecrystallized ones is <2° [24−26]. This value was adopted also in the current study. According to Figs. 5 and 6, composite reinforced with 0.92 vol.% GNPs includes the highest region fraction of blue pixels (GOS value <2°). So, the highest fraction of recrystallized grains belongs to the post-deformation annealed composite reinforced with 0.92 vol.% GNPs. The recrystallized fraction in the post-deformation annealed composite reinforced with 0.96 vol.% CNTs was lower than that of the post-deformation annealed Al7075. In composite reinforced with 0.87 vol.% (CNTs+GNPs) the lowest fraction of recrystallized grains can be seen. Therefore, it is supported that the combination of both CNTs and GNPs in the matrix can significantly inhibit recrystallization.

In spite of the sub-micrometer reinforcements which prevent the recrystallization, reinforcements (>1 μm) usually lead to stimulating the recrystallization by PSN mechanism during or after deformation [27−31]. Therefore, in the post-deformation annealed composite reinforced with 0.92 vol.% GNPs, the reinforcement (>1 μm) causes PSN.

As a result, the fraction of recrystallized grains in 0.92 vol.% GNPs reinforced composite increased compared to unreinforced Al7075. As reported in Ref. [32], distribution of reinforcements in the metal matrix can prevent grain boundary bulging and cause the crystallization to stop again by pinning the grain boundaries by Zener pining effect. Thus, in the post-deformation annealed hybrid composite the mechanism of Zener pinning effect overcame the PSN mechanism. Consequently, the fraction of the area recrystallized significantly reduced compared to the post-deformation annealed Al7075. The volume fraction of recrystallized grains through the PSN mechanisms in the vicinity of GNPs, CNTs, and the hybrid reinforcement (CNTs+GNPs) is different. The cause of this issue will be studied in the next research.

As shown in Fig. 7, in the post-deformation annealed composite reinforced with GNPs, all adjacent particle grains have recrystallized, while in CNT reinforced composite only some recrystallized grains are seen in the vicinity of CNT cluster. The

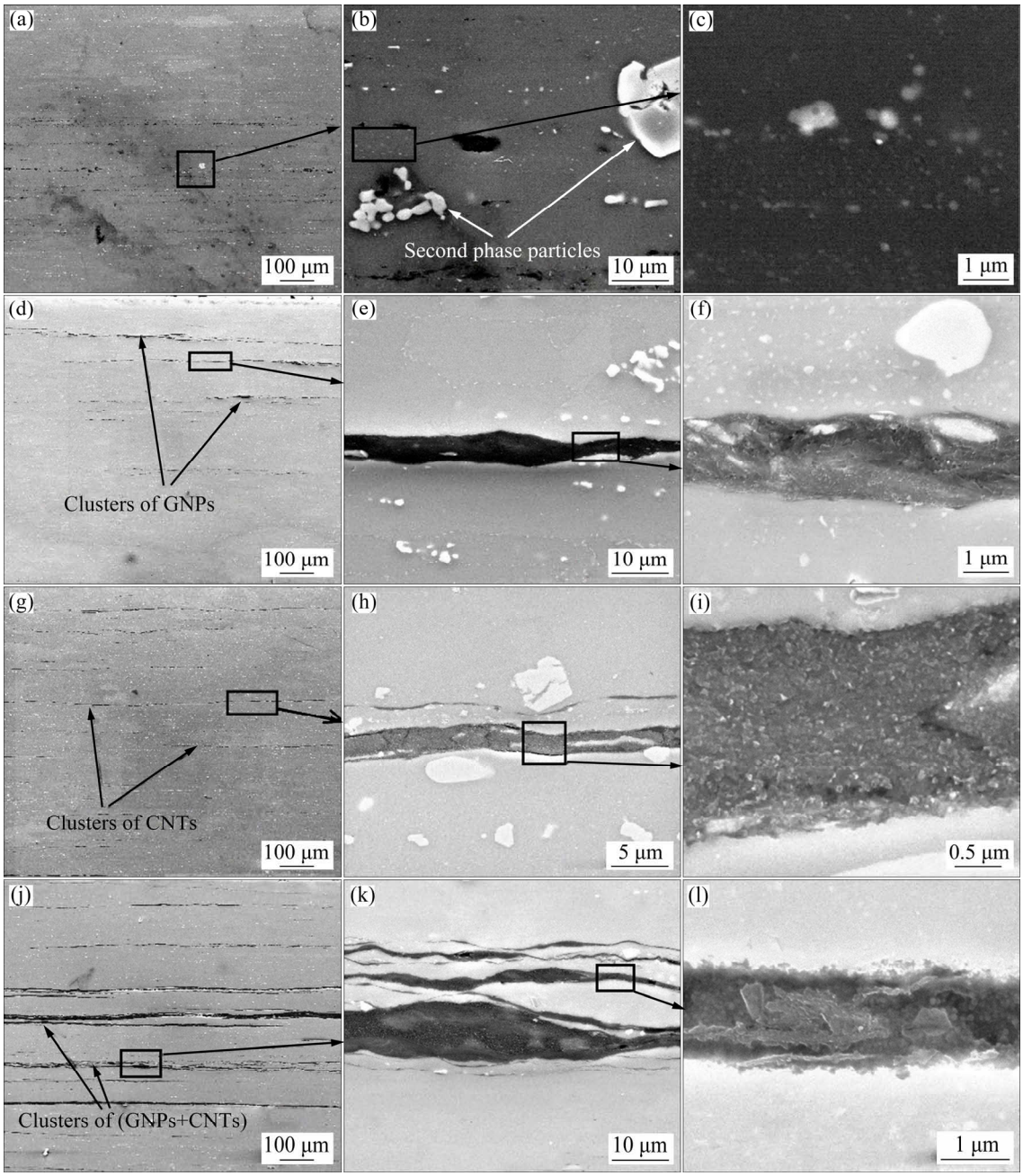

Fig. 3 SEM images of ND–RD sections of post-deformation annealed Al7075 matrix composites with different volume fractions of reinforcements: (a−c) 0; (d−f) 0.92% GNPs; (g−i) 0.96% CNTs; (j−l) 0.87% (CNTs+GNPs)

formation of recrystallized grains at the particle/matrix interface is known as PSN recrystallization nuclei. This happened during the post-deformation annealing of the hot rolled composites. In the post-deformation annealed hybrid composite, no signs of recrystallized grains are observed in the vicinity of the particles.

PSN is a mechanism of recrystallization in Al alloys containing hard reinforcing particles.

PSN has an effective role in the formation of grain structure, texture evolution and therefore affects the mechanical properties [33,34]. The effect of reinforcement particle size and shape on the occurrence of PSN has been investigated by several researchers [27−31]. Occurrence of PSN in the vicinity of intermetallic coarse particles and its effect on the microstructural properties such as texture, grain refinement and mechanical properties in the Al−Zn−Mg−Cu alloy have been investigated [33,35].

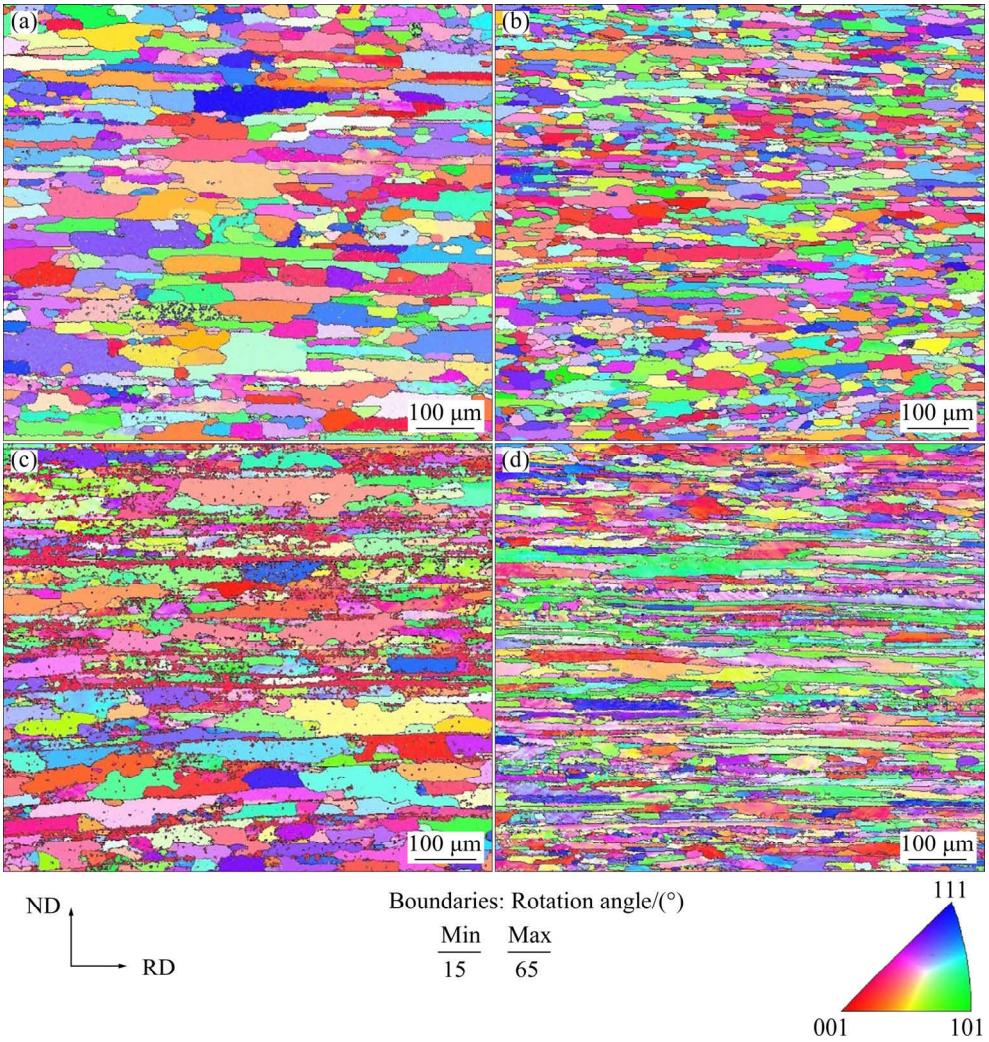

Fig. 4 Standard stereographic triangle and IPF maps measured on ND−RD sections of heat-treated Al7075 matrix composites with different volume fractions of reinforcements: (a) 0; (b) 0.92% GNPs; (c) 0.96% CNTs; (d) 0.87% (CNTs+ GNPs) (All samples are treated at the same temperatures and rolling reductions)

In Al 7xxx alloys, silicon-rich and iron-rich phases such as α-AlFeSi and Al_3Fe and particulates (>1 μm) can cause PSN [29]. The PSN nuclei form in the particle deformation zone (PDZ) next to the undeformable particulates. The PDZ is associated with a high density of dislocations and large misorientations created during deformation owing to the misfit strain between the matrix and undeformable particulates. In the PDZ, a high density of dislocations and a large incompatible strain provide the proper driving force for the nucleation of recrystallization and growth [29]. There is a relationship between the particle morphology and the shape of the PDZ formed and the strain level in the PDZ [36].

It has been reported [37] that in particles with high aspect ratio values, a larger strain gradient occurs compared to particles with lower aspect ratio values. Physically, CNTs have a positive coefficient of thermal expansion (CTE) value [38], on the other hand, GNPs have negative CTE values [39]. Due to this difference in CTE values of these two types of reinforcements a high CTE mismatch between the matrix and GNPs creates. As a result, a high density of misfit dislocations occurs during the post-deformation annealing. Thus, PDZ formed in the vicinity of GNPs is larger than that formed in the vicinity of the CNT. Accordingly, the incidence of PSN in the vicinity of GNPs is higher than that of CNTs, as seen in Fig. 7(b). During the post-deformation annealing of the hybrid composite, the combination of CNTs (with a positive CTE value) and GNPs (with a negative CTE value) can neutralize their PDZ. This reduces the driving force

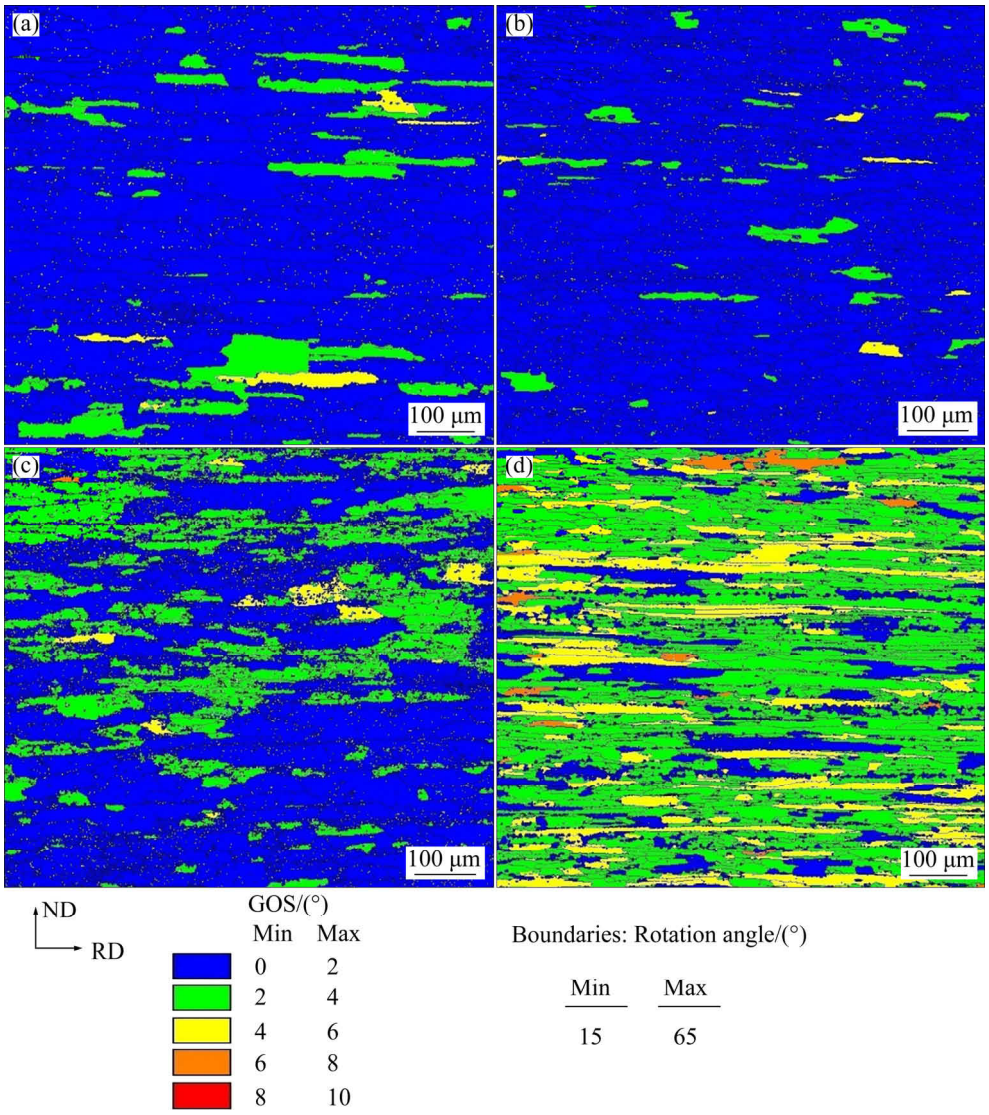

Fig. 5 GOS maps of ND–RD sections of post-deformation annealed Al7075 matrix composites with different volume fractions of reinforcements: (a) 0; (b) 0.92% GNPs; (c) 0.96% CNTs; (d) 0.87% (CNTs+GNPs)

of the occurrence of PSN in the hybrid composite, and as a result, the fraction of the recrystallized region in the hybrid composite is the lowest among other composites, as seen in Fig. 7(d)).

3.1.3 Texture evolution

Figure 8 shows the evolution of the texture of post-deformation annealed samples. The calculated main FCC fibers are shown in Fig. 9. Orientation distribution functions (ODFs) were measured under the same conditions as the IPF maps of the samples were prepared (Fig. 4).

As reported in Refs. [40,41], in as-rolled Al alloys, the significant components of the texture which are generally related to the rolling texture are S, Brass and Copper, while the main texture components related to recrystallization textures are Rotated Goss, Goss and Cube.

The presence of a strong Goss texture indicates the high formability of the material.

No research has been done on the effect of CNTs and GNPs on the texture evolution of the Al matrix composites during the post-deformation annealing process.

Addition of CNTs and GNPs to the Al7075 matrix caused different texture evolution during the post-deformation annealing, which is evaluated below. The combination of particles with different morphologies (size, shape and aspect ratio) and physical properties (deformability, immutability and hardness) affects the evolution of material texture which is related to their reaction with slip plates, dislocations and grain boundaries [32].

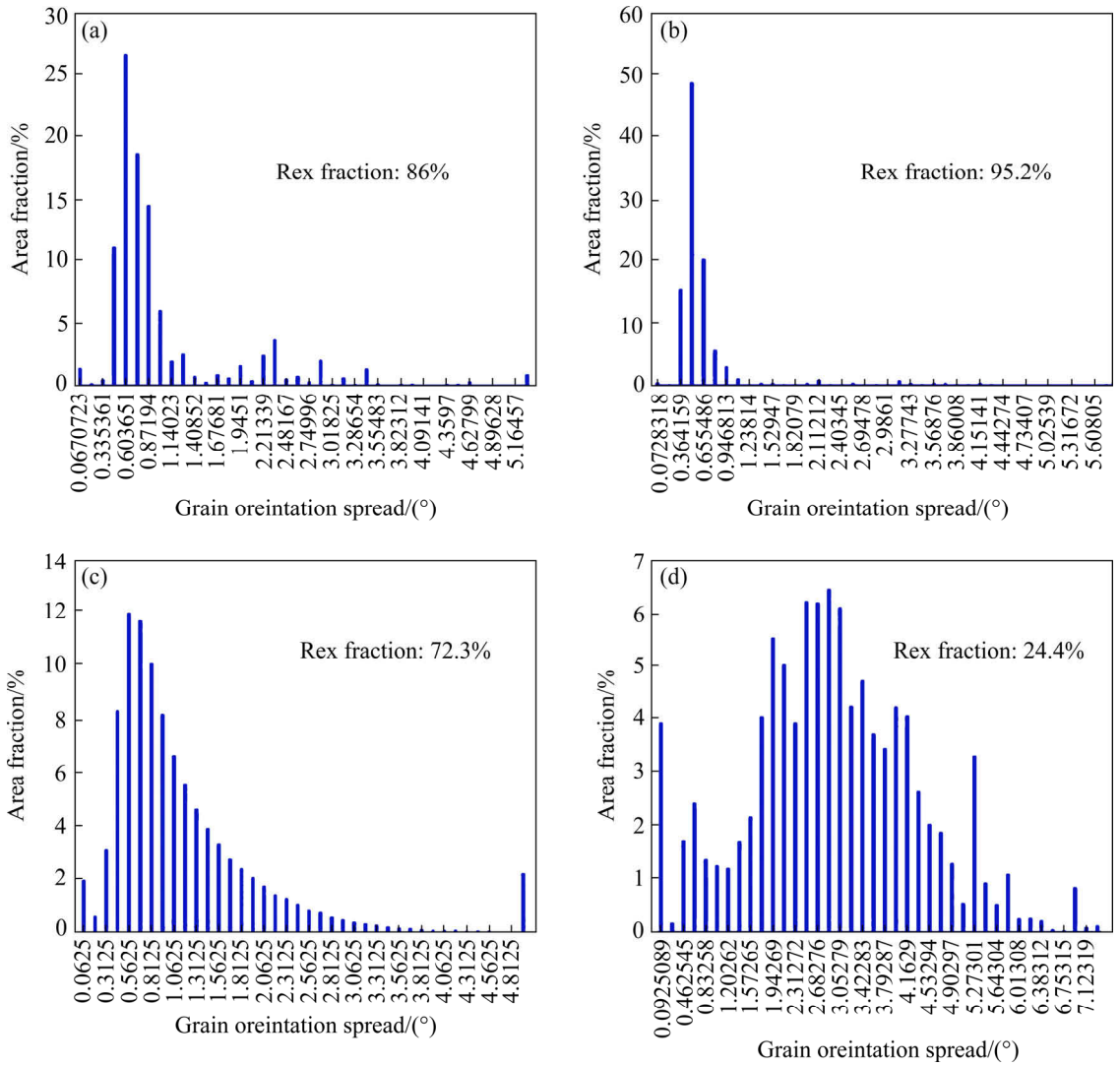

Fig. 6 GOS graphs of ND–RD sections of post-deformation annealed Al7075 matrix with different volume fractions of reinforcements: (a) 0; (b) 0.92% GNPs; (c) 0.96% CNTs; (d) 0.87% (CNTs+GNPs) (Recrystallization (rex) fractions= area fraction of grains with GOS<2°)

The exact mechanisms about the effect of CNTs and GNPs on the evolution of the matrix composite texture are still unknown. In post-deformation annealed Al7075, the main texture components are S and Dillamore (Figs. 9(b, c)). It has been reported that in deformed A3003 alloy, the main texture components are Copper and Delamore [42]. Also, it has also been observed that when Al7075 is hot rolled at 175 °C, the main texture component S is formed [43].

In reinforced composite with 0.92 vol.% GNPs, the main texture components are Copper, Rotated Cube, and Brass, and the intensity of texture components is the lowest among all samples (Figs. 9(b, c)) due to its highest recrystallized area among all samples (Figs. 5(b) and 6(b)). In the accumulative roll bonded Al−Al_2O_3−ZrC composite, the Rotated Cube was the main component of the texture [12]. In composite reinforced with 0.96 vol.% CNTs, in addition to a very strong Cube texture component, which does not appear in fibers but is quite evident in ODF plots (Fig. 8), the main components of texture are S, Copper, and Brass (Fig. 9(b)). In hybrid composite, the texture components are usually S and Brass, which are attributed to the typical texture components of deformed Al alloys. This means that the highest thermal stability of the microstructure is related to the hybrid composite whose microstructure has changed slightly during the post-deformation annealing, while the thermal stability of the composite reinforced with 0.92 vol.% GNPs was

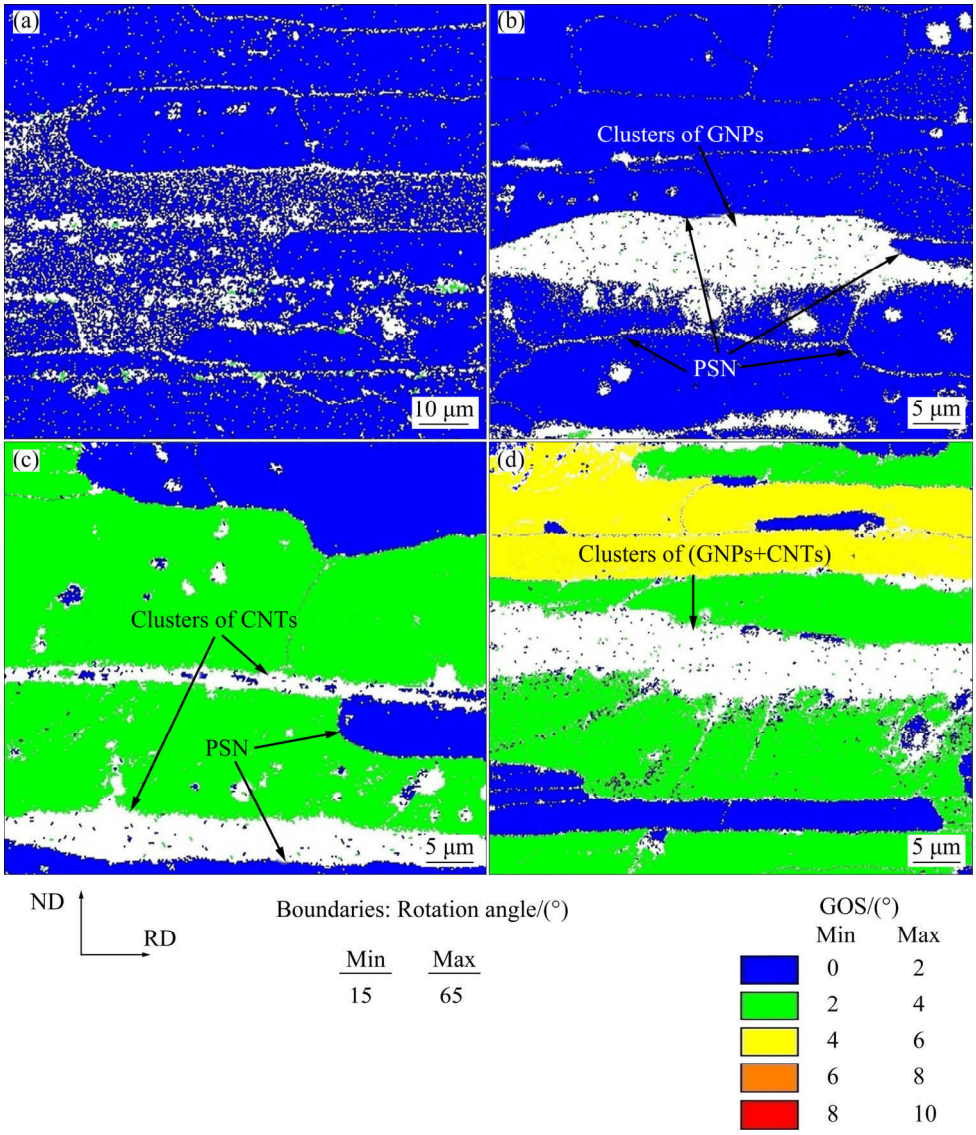

Fig. 7 GOS maps in vicinity of clustered reinforcements of post-deformation annealed Al7075 matrix composites with different volume fractions of reinforcements: (a) 0; (b) 0.92% GNPs; (c) 0.96% CNTs; (d) 0.87% (CNTs+GNPs)

the lowest. Using IPF and GOS analysis, it was confirmed that despite the 0.92 vol.% GNPs composite, in the hybrid composite, most of the grains are still pancaked and non-recrystallized during post-deformation annealing.

During post-deformation annealing, in the Al7075 alloy and in the composite reinforced with 0.92 vol.% GNPs texture evolution occurred via β and τ fibers.

The same results were obtained during the hot rolling of the Al−Mg−Si−Cu alloy [44]. In the post-deformation annealed 0.96 vol.% CNTs reinforced composite and in the hybrid composite, β fibers play the most important role in texture formation (Fig. 9(b)).

Weak textures in the post-deformation annealed composite reinforced with 0.92 vol.% GNPs are due to the occurrence of PSN as shown by GOS maps (Fig. 7).

The different orientations that are formed during rolling weaken the deformation texture and thus affect the mechanical properties [29].

The addition of SiC and CNT reinforcements into the matrix as well as the second phase precipitation during the friction stirring process weakens the texture components through the PSN mechanism and the Zener pinning effect [45]. Texture weakening can be attributed to preventing grain rotation alongside reinforcing clusters where high dislocation densities and large lattice rotations

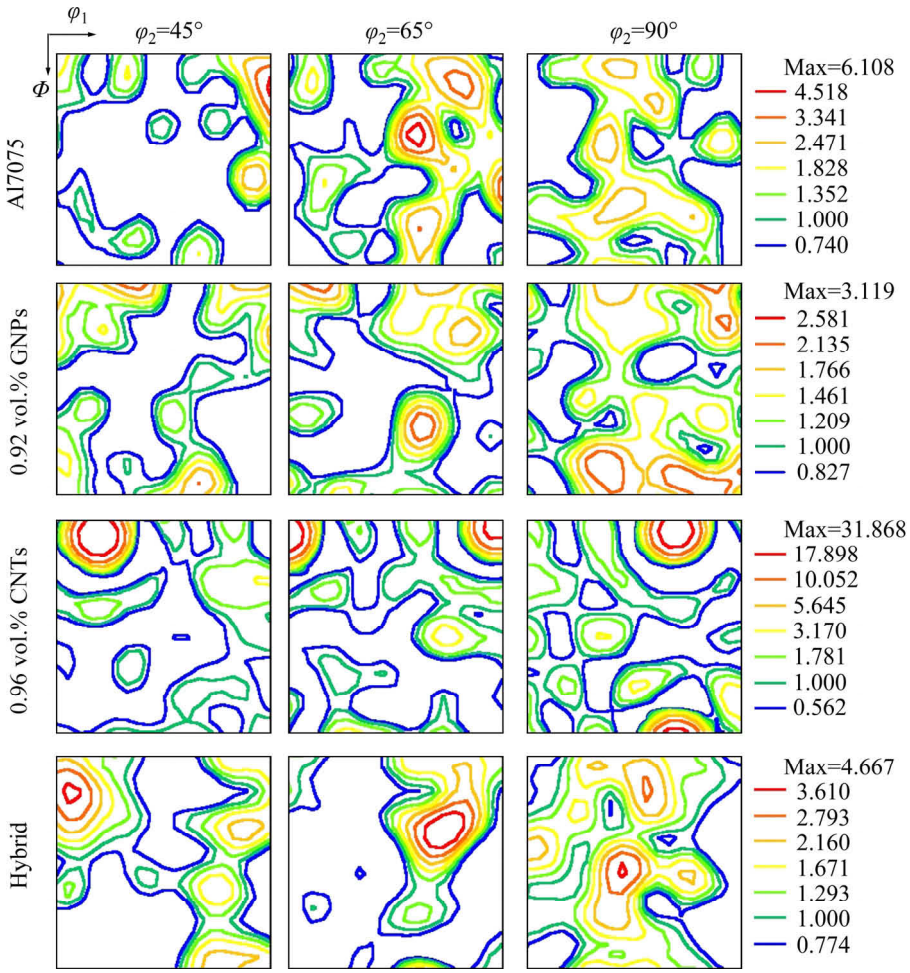

Fig. 8 ODFs of post-deformation annealed samples

occur, so grain rotation is limited. Therefore, rotation of the grains in the same orientations as the whole matrix is prohibited in such areas, thus it weakens the texture [46−48]. These are the reasons for the weakening of the texture in the 0.92 vol.% GNPs reinforced composite compared to the unreinforced Al7075.

3.2 Effect of CNTs and GNPs on hardness of processed composites

Figure 10 shows the Brinell hardness of samples subjected to post-deformation annealing. As can be seen, the hardness of the composites increases with the addition of GNPs, CNTs, and GNPs+CNTs (hybrid) in the matrix. The increasing difficulty is due to the strengthening mechanisms [49−51]. During the post-deformation annealing, the reinforcements increase the dislocation density in the matrix/interface particles for the following reasons: (1) strain incompatibility between the matrix and the reinforcements leading to the geometrically necessary dislocations at the interface (elastic modulus mismatch), (2) the difference in CTE between the matrix and the reinforcements during cooling (CTE mismatch), (3) the addition of reinforcements due to pinning of the grain boundary, accelerates grain refinement (Hall−Patch), and (4) with the presence of reinforcements in the matrix dislocation pileup occurs in their vicinity (Orowan ring) [1,10]. Another reason for the increase in hardness can be the transfer of applied load from the matrix to the reinforcements (load transfer) [49].

During the recrystallization of metals, the hardness decreases due to the elimination of dislocations [32]. Therefore, among the samples, the highest hardness due to the lowest recrystallization level belongs to the hybrid composite that is seen in Figs. 5 and 6. The hardness of 0.96 vol.% CNT reinforced composite

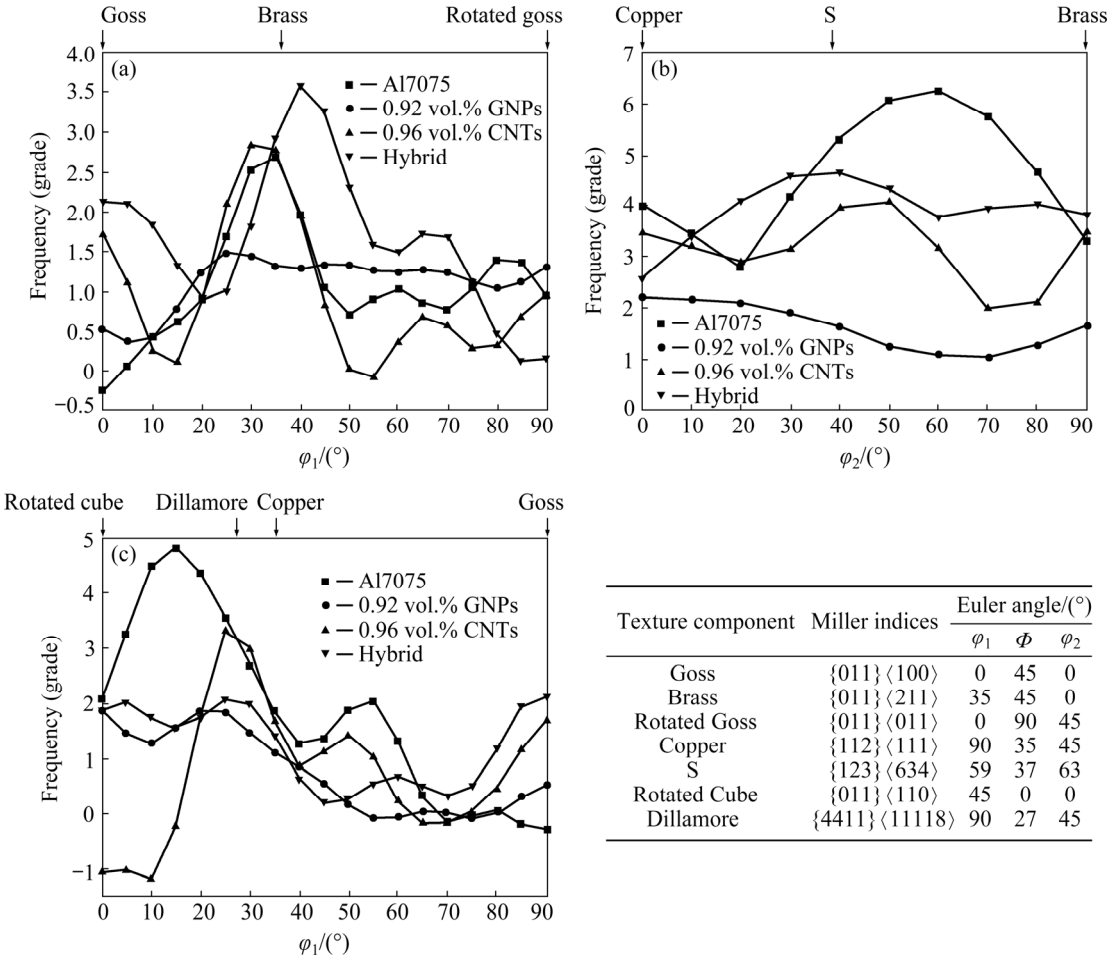

Texture component	Miller indices	Euler angle/(°)		
		φ_1	Φ	φ_2
Goss	{011}⟨100⟩	0	45	0
Brass	{011}⟨211⟩	35	45	0
Rotated Goss	{011}⟨011⟩	0	90	45
Copper	{112}⟨111⟩	90	35	45
S	{123}⟨634⟩	59	37	63
Rotated Cube	{011}⟨110⟩	45	0	0
Dillamore	{4411}⟨11118⟩	90	27	45

Fig. 9 Intensity of FCC fibers of post-deformation annealed samples: (a) α-fiber; (b) β-fiber; (c) τ-fiber

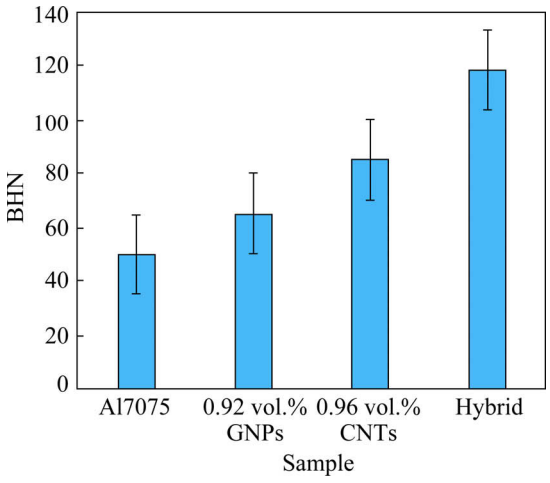

Fig. 10 Brinell hardness of post-deformation annealed samples

was lower than that of hybrid composites because the recrystallization region of 0.96 vol.% CNT reinforced composite was higher than that of hybrid composites. Although 0.92 vol.% GNP reinforced composite has the highest level of recrystallization, the hardness of 0.92 vol.% GNP reinforced composite is higher than that of unreinforced Al7075. This is because the grain size of 0.92 vol.% GNP reinforced composite (28 μm) is less than that of unreinforced Al7075 (55 μm).

By adding 1.5 wt.% nano-sized SiC to A357 alloy using electromagnetic stir casting, the hardness, yield strength and tensile strength of the prepared composite are significantly increased [52]. The presence of yttrium with grain refinement and precipitation mechanisms improves the mechanical properties of spark plasma sintered AA2024 matrix composites [53]. By incorporating GNPs in Al−Si−Cu matrix composites, mechanical properties are enhanced through dislocation strengthening, load transfer strengthening, and grain refinement strengthening mechanisms [54]. The addition of TiB_2 nanoparticles to Al−10Si−Mg using selective laser melting leads to increase of mechanical properties by grain refinement mechanism [55].

4 Conclusions

(1) EBSD data showed that fraction of the recrystallization depends on the occurrence of PSN at the reinforcements/matrix interface. GOS maps showed the occurrence of PSN in all grains in the vicinity of GNPs due to the high CTE mismatch between the GNPs and the matrix. Addition of both CNTs and GNPs in the matrix significantly resulted in the inhibition of crystallization during the post-deformation annealing.

(2) In Al7075, the main components of texture were S and Dillamore, and texture evolution occurred via β and τ fibers. In composite reinforced with 0.92 vol.% GNP, the main components of texture were Copper, Rotated Cube and Brass. In this sample, β and τ fibers play an important role in texture evolution during the post-deformation annealing process. By adding 0.96 vol.% CNTs, in addition to very strong Cube texture, the substantial components of texture including S, Copper, and Brass, and texture evolution occurred via β fiber. In the hybrid composite, which had the lowest recrystallized grains among the samples, the texture components were typically Brass and S. During the post-deformation annealing of the hybrid composite, β fiber played the most important role in texture formation.

(3) According to GOS maps and texture data, the highest microstructural thermal stability is related to hybrid composites. The thermal stability of the microstructure was the lowest in the composite reinforced with 0.92 vol.% GNP.

(4) The addition of CNTs, GNPs and hybrid reinforcements in the matrix increased the hardness and maximum hardness of the hybrid composite was due to its minimum recrystallization fraction.

Acknowledgments

The authors are grateful to the Sahand University of Technology and Ghent University for the support of this research and for the provision of research facilities used in this work.

References

[1] ALIZADEH M, GHAFFARI M, AMINI R. Properties of high specific strength Al−4wt.%Al_2O_3/B_4C nano-composite produced by accumulative roll bonding process [J]. Materials & Design, 2013, 50: 427−432.

[2] BAKSHI S R, LAHIRI D, AGARWAL A. Carbon nanotube reinforced metal matrix composites — A review [J]. International Materials Reviews, 2010, 55: 41−64.

[3] GHAZANLOU S I, AHMADIYEH S, YAVARI R. Investigation of pulse electrodeposited Ni−Co/SiO_2 nanocomposite coating [J]. Surface Engineering, 2017, 33: 337−347.

[4] GHAZANLOU S I, FARHOOD A, HOSOULI S, AHMADIYEH S, RASOOLI A. Pulse frequency and duty cycle effects on the electrodeposited Ni−Co reinforced with micro and nano-sized ZnO [J]. Journal of Materials Science: Materials in Electronics, 2017, 28: 15537−15551.

[5] IMANIAN GHAZANLOU S, FARHOOD A H S, HOSOULI S, AHMADIYEH S, RASOOLI A. Pulse and direct electrodeposition of Ni−Co/micro and nanosized SiO2 particles [J]. Materials and Manufacturing Processes, 2018, 33: 1067−1079.

[6] HASHEMI M, JAMAATI R, TOROGHINEJAD M R. Microstructure and mechanical properties of Al/SiO_2 composite produced by CAR process [J]. Materials Science and Engineering A, 2012, 532: 275−281.

[7] UTHAYAKUMAR M, ARAVINDAN S, RAJKUMAR K. Wear performance of Al–SiC–B_4C hybrid composites under dry sliding conditions [J]. Materials & Design, 2013, 47: 456−464.

[8] ALIZADEH M, GHAFFARI M, AMINI R. Investigation of grain refinement in Al/Al_2O_3/B_4C nano-composite produced by ARB [J]. Composites Part B: Engineering, 2014, 58: 438−442.

[9] FEI W D, LI W Z, YAO C K. Hot rolling behaviors of whisker reinforced aluminum composites [J]. Journal of Materials Science, 2002, 37: 211−215.

[10] NASERI M, HASSANI A, TAJALLY M. An alternative method for manufacturing Al/B_4C/SiC hybrid composite strips by cross accumulative roll bonding (CARB) process [J]. Ceramics International, 2015, 41: 13461−13469.

[11] REIHANIAN M, LARI BAGHAL S M, KESHAVARZ HADDADIAN F, PAYDAR M H. A comparative corrosion study of Al/Al_2O_3-SiC hybrid composite fabricated by accumulative roll bonding (ARB) [J] Journal of Ultrafine Grained and Nanostructured Materials, 2016, 49: 29−35.

[12] SHAMANIAN M, MOHAMMADNEZHAD M, ASGARI H, SZPUNAR J. Fabrication and characterization of Al–Al_2O_3–ZrC composite produced by accumulative roll bonding (ARB) process [J]. Journal of Alloys and Compounds, 2015, 618: 19−26.

[13] GUO B S, NI S, YI J H, SHEN R J, TANG Z H, DU Y M. Microstructures and mechanical properties of carbon nanotubes reinforced pure aluminum composites synthesized by spark plasma sintering and hot rolling [J]. Materials Science and Engineering A, 2017, 698: 282−288.

[14] KWON H, KAWASAKI A. Extrusion of spark plasma sintered aluminum-carbon nanotube composites at various sintering temperatures [J]. Journal of Nanoscience and Nanotechnology, 2009, 9: 6542−6548.

[15] KWON H, PARK D H, SILVAIN J F, KAWASAKI A. Investigation of carbon nanotube reinforced aluminum matrix composite materials [J]. Composites Science and Technology, 2010, 70: 546−550.

[16] TABRIZI S G, SAJJADI S A, BABAKHANI A, LU W. Influence of spark plasma sintering and subsequent hot rolling on microstructure and flexural behavior of in-situ TiB and TiC reinforced Ti6Al4V composite [J]. Materials Science and Engineering A, 2015, 624: 271−278.

[17] NOVOSELOV K S, GEIM A K, MOROZOV S V, JIANG D, ZHANG Y, DUBONOS S V. Electric field effect in atomically thin carbon films [J]. Science, 2004, 306: 666−669.

[18] LEE C, WEI X, KYSAR J W, HONE J. Measurement of the elastic properties and intrinsic strength of monolayer graphene [J]. Science, 2008, 321: 385−388.

[19] BALANDIN A A. Thermal properties of graphene and nanostructured carbon materials [J]. Nature Materials, 2011, 10: 569−581.

[20] LI J L, XIONG Y C, WANG X D, YAN S J, YANG C H, HE W W, CHEN J Z, WANG S Q, ZHANG X Y, DAI S L. Microstructure and tensile properties of bulk nanostructured aluminum/graphene composites prepared via cryomilling [J]. Materials Science and Engineering: A, 2015, 626: 400−405.

[21] YAN S J, DAI S L, ZHANG X Y, YANG C, HONG Q H, CHEN J Z, LIN Z M. Investigating aluminum alloy reinforced by graphene nanoflakes [J]. Materials Science and Engineering A, 2014, 612: 440−444.

[22] SABOORI A, PAVESE M, BADINI C, FINO P. Microstructure and thermal conductivity of Al–Graphene composites fabricated by powder metallurgy and hot rolling techniques [J]. Acta Metallurgica Sinica (English Letters), 2017, 30: 675−687.

[23] GHAZANLOU S I, EGHBAI B. Fabrication and characterization of GNPs and CNTs reinforced Al7075 matrix composites through stir casting process [J]. International Journal of Minerals, Metallurgy and Materials, 2021, 28: 1204−1214.

[24] HADADZADEH A, MOKDAD F, WELLS M, CHEN D. A new grain orientation spread approach to analyze the dynamic recrystallization behavior of a cast-homogenized Mg−Zn−Zr alloy using electron backscattered diffraction [J]. Materials Science and Engineering A, 2018, 709: 285−289.

[25] LIAO B, CAO L, WU X, ZOU Y, HUANG G, ROMETESCH P. A. Effect of post-deformation annealing condition on the flow behavior and recrystallization mechanisms of aluminum alloy 7055 [J]. Materials, 2019, 12: 311.

[26] GHAZANLOU S I, EGHBALI B, PETROV R. Study on the microstructural and evolution of texture of hot rolled Al7075/graphene/carbon nanotubes reinforced composites [J]. Materials Chemistry and Physics, 2021, 257: 123766.

[27] ADAM K F, LONG Z, FIELD D P. Analysis of particle-stimulated nucleation (PSN)-dominated recrystallization for hot-rolled 7050 aluminum alloy [J]. Metallurgical and Materials Transactions A, 2017, 48: 2062−2076.

[28] LI Z, JIANG H, WANG Y, ZHANG D, YAN D, RONG L. Effect of minor Sc addition on microstructure and stress corrosion cracking behavior of medium strength Al–Zn–Mg alloy [J]. Journal of Materials Science & Technology, 2018. 34: 1172−1179.

[29] SHE H, SHU D, DONG A P, WANG J, SUN B D, LAI H C. Relationship of particle stimulated nucleation, recrystallization and mechanical properties responding to Fe and Si contents in hot-extruded 7055 aluminum alloys [J]. Journal of Materials Science & Technology, 2019, 35: 2570−2581.

[30] TSIVOULAS D, PRANGNELL P. The effect of Mn and Zr dispersoid-forming additions on recrystallization resistance in Al−Cu−Li AA2198 sheet [J]. Acta Materialia, 2014, 77: 1−16.

[31] WANG Y, ZHANG Z, WU R Z, SUN J F, JIAO Y L, HOU L G, ZHANG J H, LI X L, ZHANG M L. Ambient-temperature mechanical properties of isochronally aged 1420-Sc−Zr aluminum alloy [J]. Materials Science and Engineering A, 2019, 745: 411−419.

[32] HUMPHREYS F J, HATHERLY M. Recrystallization and related annealing phenomena [M]. Elsevier, 2012.

[33] FANG H C, LUO F H, CHEN K H. Effect of intermetallic phases and recrystallization on the corrosion and fracture behavior of an Al−Zn−Mg−Cu−Zr−Yb−Cr alloy [J]. Materials Science and Engineering A, 2017, 684: 480−490.

[34] ZHAO Q L, ZHANG H D, HUANG K, MARTHINSEN K. Correlating oriented grain number density of recrystallisation in particle-reinforced with aluminium alloys [J]. Transactions of Nonferrous Metals Society of China, 2018, 28: 220−225.

[35] LI X, STARINK M. DSC study on phase transitions and their correlation with properties of overaged Al−Zn−Mg−Cu alloys [J]. Journal of Materials Engineering and Performance, 2012, 21: 977−984.

[36] SCHAFER C, SONG J, GOTTSTEIN G. Modeling of evolution of texture in the deformation zone of second-phase particles [J]. Acta Materialia, 2009, 57: 1026−1034.

[37] SIDOR J J, DECROOS K, PETROV R. H, KESTENS L A. Evolution of recrystallization textures in particle reinforced with Al alloys after various rolling reductions: Experimental study and modeling [J]. International Journal of Plasticity, 2015, 66: 119−137.

[38] PARK J G, KEUM D H, LEE Y H. Strengthening mechanisms in carbon nanotube-reinforced aluminum composites [J]. Carbon, 2015, 95: 690−698.

[39] ZHANG D, ZHAN Z. Strengthening effect of graphene derivatives in copper matrix composites [J]. Journal of Alloys and Compounds, 2016, 654: 226−233.

[40] BAREKAR N, DAS S, YANG X, HUANG Y, EL FAKIR O, BHAGURKAR A. The impact of melt conditioning on microstructure, texture and ductility of twin roll cast aluminium alloy strips [J]. Materials Science and Engineering A, 2016, 650: 365−373.

[41] NASERI M, REIHANIAN M, BORHANI E. EBSD characterization of nano/ultrafine structured Al/Brass composite produced by severe plastic deformation [J]. Journal of Ultrafine Grained and Nanostructured Materials, 2018, 51: 123−138.

[42] PIRGAZI H, AKBARZADEH A, PETROV R, SIDOR J, KESTENS L. Evolution of texture of AA3003 aluminum alloy sheet produced by accumulative roll bonding [J]. Materials Science and Engineering A, 2008, 492: 110−117.

[43] CAPEDA-JIMENEZ C, POZUELO M, RUANO O A, CARRENO F. Influence of the thermal treatment on the microstructure and hardness evolution of 7075 aluminium layers in a hot-rolled multilayer laminate composite [J].

Journal of Alloys and Compounds, 2009, 478: 154−162.
[44] WANG Y H, ZHANG L X, YANG X H, LI K, NI S, DU Y, SONG M. Texture/microstructural evolution and mechanical properties of a hot and cold rolled Al−Mg−Si−Cu alloy [J]. Journal of Minerals and Materials Characterization and Engineering, 2017, 5: 209−222.
[45] JIAN V K S, YAZAR K, MUTHUKUMARAN S. Development and characterization of Al5083-CNTs/SiC composites via friction stir processing [J]. Journal of Alloys and Compounds, 2019, 798: 82−92.
[46] HIDALGO-MANRIQUE P, YAN S, LIN F, HONG Q, KINLOCH I A, CHEN X. Microstructure and mechanical behaviour of aluminium matrix composites reinforced with graphene oxide and carbon nanotubes [J]. Journal of Materials Science, 2017, 52: 13466−13477.
[47] HUMPHREYS F, KALU P. The plasticity of particle-reinforced with polycrystals [J]. Acta Metallurgica et Materialia, 1990, 38: 917−930.
[48] JIANG X, GALANO M, AUDEBERT F. Extrusion textures in Al, 6061 alloy and 6061/SiC_p nanocomposites [J]. Materials Characterization, 2014, 88: 111−118.
[49] KIM C S, CHO K, MANJILI M H, NEZAFATI M. Mechanical performance of particulate-reinforced Al metal-matrix composites (MMCs) and Al metal-matrix nano-composites (MMNCs) [J]. Journal of Materials Science, 2017, 52: 13319−13349.
[50] SANATY-ZADEH A. Comparison between current models for the strength of particulate-reinforced metal matrix nanocomposites with emphasis on consideration of Hall–Petch effect [J]. Materials Science and Engineering A, 2012, 531: 112−118.
[51] YUAN Q H, QIU Z Q, ZHOU G H, ZENG X S, LUO L, RAO X X. Interfacial design and strengthening mechanisms of AZ91 alloy reinforced with in-situ reduced graphene oxide [J]. Materials Characterization, 2018, 138: 215−228.
[52] BADIZI R M, PARIZAD A, ASKARI-PAYKANI M, SHAHVERDI H R. Optimization of mechanical properties using D-optimal factorial design of experiment: Electromagnetic stir casting process of A357−SiC nanocomposite [J]. Transactions of Nonferrous Metals Society of China, 2020, 30: 1183−1194.
[53] VIDYASAGAR C. S, KARUNAKAR D. Characterization of mechanical properties and microstructures of spark plasma sintered and cryo-rolled AA2024−Y composites [J]. Transactions of Nonferrous Metals Society of China, 2020, 30: 1439−1451.
[54] XIONG J J, HONG Y. Microstructure and mechanical properties of ADC12 composites reinforced with graphene nanoplates prepared by ultrasonic assisted casting [J]. Transactions of Nonferrous Metals Society of China, 2020, 30: 3210−3225.
[55] PEI W, ECKERT J, PRASHANTH K G, WU M W, KABAN I, XI L X. A review of particulate-reinforced aluminum matrix composites fabricated by selective laser melting [J]. Transactions of Nonferrous Metals Society of China, 2020, 30: 2001−2034.

EBSD 表征变形后退火 Al7075/石墨烯纳米片/碳纳米管复合材料

Siavash IMANIAN GHAZANLOU[1], Baitallah EGHBALI[1], Roumen PETROV[2,3]

1. Faculty of Materials Engineering, Sahand University of Technology, P. O. Box: 51335-1996, Tabriz, Iran;
2. Department of Electromechanical Systems and Metal Engineering, Research Group Materials Science and Technology, Ghent University, Tech Lane Science Park Campus A, 46, 9062 Gent, Belgium;
3. Department of Materials Science and Engineering, Delft University of Technology, Mekelweg 2, Delft, The Netherlands

摘　要：研究变形后退火对碳纳米管(CNTs)和石墨烯纳米片(GNPs)增强热轧 Al7075 基复合材料显微组织演变的影响。对搅拌铸造样品进行多道次热轧，然后在 450 °C 下退火 4 h。采用 SEM、EDS 和 EBSD 技术观察材料的显微组织演变。EBSD 数据显示，添加体积分数(下同)为 0.87%的 GNPs 和 CNTs 可明显抑制再结晶的发生。当添加 0.96%的 CNTs 时，再结晶受到部分抑制。而当添加 0.92%的 GNPs 时，明显加快了粒子激发形核(PSN)机制导致的再结晶。在有增强相存在的情况下，再结晶晶粒的体积分数与 PSN 的产生有显著的关系。主要织构的强度和类型都取决于增强相的种类。

关键词：退火；复合材料；石墨烯纳米片；碳纳米管；再结晶；粒子激发形核；织构

(Edited by Xiang-qun LI)